Magnetization transfer MR imaging to monitor muscle tissue formation during myogenic in vivo differentiation of muscle precursor cells

Rottmar, Markus ; Haralampieva, Deana ; Salemi, Souzan ; Eberhardt, Christian ; Wurnig, Moritz C ; Boss, Andreas ; Eberli, Daniel

Abstract: Purpose To determine whether magnetization transfer (MT) magnetic resonance (MR) imaging may serve as a quantitative measure of the degree of fiber formation during differentiation of muscle precursor cells into engineered muscle tissue as a potential noninvasive monitoring tool in mice. Materials and Methods The study was approved by the local ethics committee (no. StV 01/2008) and the local Veterinary Office (license no. 99/2013). Human muscle progenitor cells (hMPCs) derived from rectus abdominis muscles were subcutaneously injected into CD-1 nude mice (CD-1 nude mice, Crl:CD1-Foxn1(nu); Charles River Laboratories, Wilmington, Mass) for development of muscle tissue. The mice underwent MR imaging examinations at 4.7 T at days 1, 3, 7, 14, 21, and 28 after cell transplantation by using a gradient-echo sequence with an MT prepulse and systematic variation of the off-resonance frequency (50-37 500 Hz) at an amplitude of 800°. Direct saturation was estimated from a Bloch equation simulation. The MT ratio (MTR) was correlated to immunohistochemistry findings, Western blot results, and results of myography. Data were analyzed by using one-way or two-way analysis of variance with the Sidak or Tukey multiple comparisons test. Results In the reference skeletal muscle, highest MT was found for 2500 Hz off-resonance frequency with an MTR ± standard deviation of 57.5% ± 3.5. The developing muscle tissue exhibited increasing MT values during the 28 days of myogenic in vivo differentiation and did not reach the values of native skeletal muscle. Mean values of MTR (2500 Hz) for hMPCs were 27.6% ± 6.3 (day 1), 24.7% ± 8.7 (day 3), 28.2% ± 5.7 (day 7), 35.9% ± 5.0 (day 14), 37.0% ± 7.9 (day 21), and 39.9% ± 8.1 (day 28). The results from MT MR imaging correlated qualitatively well with muscle tissue expression of specific skeletal markers, as well as muscle contractility. Conclusion MT MR imaging may be used to noninvasively monitor the process of myogenic in vivo differentiation of hMPCs as a biomarker of the quantity and quality of muscle fiber formation. (©) RSNA, 2016 Online supplemental material is available for this article.

DOI: https://doi.org/10.1148/radiol.2016152330

Radiology

Magnetization Transfer MR Imaging to Monitor Muscle Tissue Formation during Myogenic in Vivo Differentiation of Muscle Precursor Cells[1]

Markus Rottmar, PhD
Deana Haralampieva, PhD
Souzan Salemi, PhD
Christian Eberhardt, PhD
Moritz C. Wurnig, MD, MSc
Andreas Boss, MD, PhD
Daniel Eberli, MD, PhD

Purpose: To determine whether magnetization transfer (MT) magnetic resonance (MR) imaging may serve as a quantitative measure of the degree of fiber formation during differentiation of muscle precursor cells into engineered muscle tissue as a potential noninvasive monitoring tool in mice.

Materials and Methods: The study was approved by the local ethics committee (no. StV 01/2008) and the local Veterinary Office (license no. 99/2013). Human muscle progenitor cells (hMPCs) derived from rectus abdominis muscles were subcutaneously injected into CD-1 nude mice (CD-1 nude mice, Crl:CD1-Foxn1^{nu}; Charles River Laboratories, Wilmington, Mass) for development of muscle tissue. The mice underwent MR imaging examinations at 4.7 T at days 1, 3, 7, 14, 21, and 28 after cell transplantation by using a gradient-echo sequence with an MT prepulse and systematic variation of the off-resonance frequency (50–37 500 Hz) at an amplitude of 800°. Direct saturation was estimated from a Bloch equation simulation. The MT ratio (MTR) was correlated to immunohistochemistry findings, Western blot results, and results of myography. Data were analyzed by using one-way or two-way analysis of variance with the Sidak or Tukey multiple comparisons test.

Results: In the reference skeletal muscle, highest MT was found for 2500 Hz off-resonance frequency with an MTR ± standard deviation of 57.5% ± 3.5. The developing muscle tissue exhibited increasing MT values during the 28 days of myogenic in vivo differentiation and did not reach the values of native skeletal muscle. Mean values of MTR (2500 Hz) for hMPCs were 27.6% ± 6.3 (day 1), 24.7% ± 8.7 (day 3), 28.2% ± 5.7 (day 7), 35.9% ± 5.0 (day 14), 37.0% ± 7.9 (day 21), and 39.9% ± 8.1 (day 28). The results from MT MR imaging correlated qualitatively well with muscle tissue expression of specific skeletal markers, as well as muscle contractility.

Conclusion: MT MR imaging may be used to noninvasively monitor the process of myogenic in vivo differentiation of hMPCs as a biomarker of the quantity and quality of muscle fiber formation.

Online supplemental material is available for this article.

[1] From the Institute of Diagnostic and Interventional Radiology (M.R., C.E., M.C.W., A.B.) and Department of Urology (M.R., D.H., S.S., D.E.), University Hospital Zurich, Rämistrasse 100, CH-8091 Zurich, Switzerland; and Laboratory for Biointerfaces, Empa, Swiss Federal Laboratories for Materials Science and Technology, St Gallen, Switzerland (M.R.). Received November 2, 2015; revision requested December 14; final revision received February 10, 2016; accepted February 29; final version accepted March 9. **Address correspondence to** A.B. (e-mail: andreas.boss@usz.ch).

A.B. and D.E. contributed equally to this work.

Study supported by Clinical Research Priority Program Molecular Imaging Zurich.

The quality of life of patients with urinary incontinence is markedly compromised (1). A conservative estimate is that urinary incontinence affects approximately 20% of women, but in fact, the prevalence may be as high as 50% in elderly women (2). Care of patients with urinary incontinence incurs annual direct costs of $16 billion in the United States (3), and demographic changes will increase the economic burden posed to society. Current treatment options for urinary incontinence show great patient-to-patient variability and only limited success overall (1).

Cell-based therapies have been proposed as a method to achieve restoration of numerous urogenital tissues and organs (4–6), with the transplantation of muscle progenitor cells (MPCs) having shown great potential as a treatment for genetic and acquired muscle disorders (7,8). Investigations on the injection of in vitro culture–expanded MPCs for the treatment of urinary incontinence in small animal models were promising (9,10), with results obtained in dogs demonstrating that MPCs are able to restore otherwise irreversibly damaged sphincter function (11). Also, research on the use of MPCs demonstrated a clinical improvement in patients with urinary incontinence, and none of the patients showed signs of rejection (12). Unfortunately, the success of such a cell therapy approach is difficult to evaluate, as it relies on indirect measures, including pre- and postinjection pad tests, a diary of incontinence episodes, and quality of life surveys.

Strategies to directly evaluate cell therapies include biopsies, as well as several imaging modalities, including optical imaging, radionuclide imaging, and magnetic resonance (MR) imaging (13). While biopsies provide tissue samples that can be analyzed histologically, they are invasive procedures that offer limited sample size. The aforementioned imaging modalities can noninvasively image the entire newly formed tissue over time. However, they generally require direct or indirect labeling of the cells to be injected (13). In MR imaging, it has been shown that MPCs can be monitored over time when labeled with magnetic nanoparticles (14,15). While the signal void artifact produced by the magnetic nanoparticles enables the assessment of cell engraftment, it inherently prevents monitoring of MR-specific tissue properties.

Muscle tissue exhibits numerous traits on MR images that are highly specific for this particular tissue type (16,17). In a recent study, the development of nonlabeled MPCs into adult skeletal muscle tissue was monitored by measuring relaxation and diffusion properties, which demonstrated that the maturing tissue develops MR characteristics similar to those of mature skeletal muscle (18). While these parameters indirectly show the degree and correct direction of differentiation, as well as viability of the MPCs during tissue formation, they lack quantitative information on the degree of fiber formation.

It has been shown previously that magnetization transfer (MT) imaging is not only a valuable method to monitor diseases such as multiple sclerosis (19,20) or bowel fibrosis in Crohn disease (21), but it can also be used to evaluate important aspects of muscle tissue formation and structure, as well as associated diseases (19,22).

The aim of our study was to determine whether MT MR imaging may serve as a quantitative measure of the degree of fiber formation during differentiation of muscle precursor cells into engineered muscle tissue as a potential noninvasive monitoring tool in mice.

Advances in Knowledge

- In developing muscle tissue, decreasing signal intensity when applying a magnetization transfer (MT) prepulse can be observed from day 1 to day 28.
- Evaluation of the MT ratio of the developing muscle tissue showed that values reached a plateau on day 21, being, at an offset frequency of 1750 Hz, 70% of the skeletal muscle reference, with little to no increase by day 28.
- Calculation of the true MT (MT_{true}) from experimental results by using numerical simulations showed that, after an initial peak at day 1, maximum MT_{true} increased over time, with 27.6% at 750 Hz, 28.4% at 750 Hz, 32.0% at 2500 Hz, 32.2% at 2500 Hz, and 33.9% at 2500 Hz at days 3, 7, 14, 21, and 28, respectively.

Materials and Methods

Study Design

Human MPCs (hMPCs) were subcutaneously injected at the back of nude mice and examined via MR imaging after 1, 3, 7, 14, 21, and 28 days, with subsequent tissue harvest at days 14 and 28 for immunohistochemistry analysis; hematoxylin-eosin and Masson trichrome staining at days 7, 14, and 28 for Western blot analysis; and myography at day 28. The number of mice comprised 17 animals for three experimental series for MT imaging (n = 6, n = 5, and n = 6), two additional mice for Western blot analysis only, and four additional mice for organ bath. Each experimental assay (histologic examination, Western blot analysis, and

Published online before print
10.1148/radiol.2016152330 **Content codes:** GU MR

Radiology 2016; 000:1–8

Abbreviations:
hMPC = human MPC
MPC = muscle progenitor cell
MT = magnetization transfer
MTR = MT ratio
MT_{true} = true MT
MyHC = myosin heavy chain

Author contributions:
Guarantors of integrity of entire study, A.B., D.E.; study concepts/study design or data acquisition or data analysis/interpretation, all authors; manuscript drafting or manuscript revision for important intellectual content, all authors; approval of final version of submitted manuscript, all authors; agrees to ensure any questions related to the work are appropriately resolved, all authors; literature research, M.R., C.E., M.C.W., A.B.; clinical studies, C.E.; experimental studies, M.R., D.H., S.S., C.E., M.C.W., A.B.; statistical analysis, M.R., C.E., M.C.W., A.B., D.E.; and manuscript editing, all authors

Conflicts of interest are listed at the end of this article.

organ bath) was performed at least three times. All animal experiments were approved by the local veterinary authorities (Veterinary Office of the Department of Health of the Canton of Zurich, license no. 99/2013).

Cell Culture

hMPCs were derived from rectus abdominis muscle samples obtained from patients undergoing abdominal surgery after providing informed consent, which was approved by the local ethics committee (ethics committee of the Canton of Zurich, no. StV 01/2008). The cells were isolated and cultured according to protocols described previously (11,23). In brief, muscle biopsy samples were minced and digested for 40 minutes at 37°C and 5% CO_2 in Dulbecco's Modified Eagle's Medium (Gibco, Grand Island, NY) and F12 nutrient mixture (Invitrogen, Carlsbad, Calif) supplemented with 0.4% dispase (Gibco) and 0.2% collagenase type I (Worthington Biochemical, Lakewood, NJ). To reduce the number of fast-adhering fibroblasts, the digested samples were centrifuged, filtered, and plated on collagen type I coated six-well dishes for 24 hours before transferring the hMPC-containing suspension to fresh collagen type I coated six-well dishes. The cells were cultivated at 37°C and 5% CO_2 with growth medium (Dulbecco's Modified Eagle's Medium [Gibco] and F12 nutrient mixture [Invitrogen]); supplemented with 18% fetal bovine serum (Gibco and Invitrogen), 1% penicillin and streptomycin (Gibco and Invitrogen), 10 μg/mL human epidermal growth factor (Sigma, Buch, Switzerland), 1 μg/mL human basic fibroblast growth factor (Sigma), 10 μg/mL human insulin (Sigma), and 0.4 μg/mL dexamethasone (Sigma); and harvested and subcultivated on standard tissue culture polystyrene dishes when reaching 80%–90% confluency.

Cell Injection

hMPCs were injected into the subcutaneous space of the back of female nude mice (CD-1 nude mice, Crl:CD1-Foxn-1^{nu}; Charles River Laboratories, Wilmington, Mass). Prior to the injection, the cells were subcultivated three times (passage 3) after initial isolation, washed with phosphate-buffered saline (Gibco and Invitrogen), and suspended in 1.5% collagen type I solution (BD Biosciences, Two Oak Park, Bedford, Mass). Animals were anesthetized with 3% isoflurane (1-Chlor-2,2,2-trifluorethyl-difluoromethylether; Attane, Minrad, Buffalo, NY), and 3×10^7 hMPCs were injected on the left and right sides of the lower back of the nude mice.

MR Imaging

Mice were subjected to MR imaging analysis 1, 3, 7, 14, 21, and 28 days after hMPC transplantation. During the imaging process, mice were anesthetized with 1.5% isoflurane. All measurements were performed with a Bruker 4.7-T Pharmascan 47/16 unit (Bruker BioSpin MRI, Ettlingen, Germany) equipped with a linear polarized hydrogen 1 mouse whole-body transmit-receive radiofrequency coil. After a gradient-echo localizer image was acquired in three spatial directions, the T2-weighted morphologic MR images were acquired by using a rapid acquisition with relaxation enhancement sequence (repetition time [msec]/echo time [msec], 2500/11; rapid acquisition with relaxation enhancement factor, eight; number of signals acquired, three; section thickness, 1 mm; field of view, 40 × 40 mm; matrix, 256 × 256; and acquisition time, 4 minutes). For MT measurements, a three-dimensional spoiled gradient-echo sequence (fast low-angle shot; 20.4/4.7; number of signals acquired, two; field of view, 40 × 30 × 30 mm; matrix, 128 × 128 × 64; spatial resolution, 0.31 × 0.23 × 0.47; excitation flip angle, 12°; receiver bandwidth, 50000 Hz; sinc excitation pulse, 1 msec; and acquisition time, 5 minutes 35 seconds) was applied with and without a systematic variation of the MT prepulse (Gaussian pulse shape, applied for each repetition time; off-resonance frequency, 50–37500 Hz; flip angle, 800°; duration, 10.9 msec; bandwidth, 250 Hz; no dummy pulses). For the validation of the MT protocol and the sequence simulation, the same three-dimensional spoiled gradient-echo sequence was used with and without a systematic variation of the MT prepulse (off-resonance frequency, 10–100000 Hz; and flip angles of 300°, 600°, 1200°, or 2400°).

Calculation of the MT Ratio and Simulation of Direct Saturation Effects

The MT ratio (MTR), calculated as MTR = $(M_0 - M_{SAT})/M_0$, where M_0 represents the equilibrium magnetization (MR signal intensity) without MT pulse and M_{SAT} represents the magnetization with MT prepulse, was calculated as a quantitative measure of the interaction of the macromolecular pool with the liquid pool. MTR values from the acquired images were calculated pixelwise on a stand-alone computer by using an in-house–developed routine written in the Matlab programming language (MathWorks, Natick, Mass). Since the injected collagen and cell volume showed a strong decrease over time, drawing of a reasonable region of interest for MTR evaluation was not possible in all animals or for all injections. For MTR analysis, 15 injections in eight mice fulfilled this criterion at day 21, and eight injections in four mice fulfilled this criterion at day 28. Simulation of direct saturation effects was performed by using a custom-written C++ program (kindly provided by Fritz Schick, University Hospital Tübingen, Tübingen, Germany) as described previously (24). On the basis of the settings obtained from the MR imaging unit, the used routine encompassed a wait time of 115 μsec, followed by a radiofrequency pulse (Gaussian shape, 800° angle, and 10.9-msec duration, directly followed by a 226-μsec MT spoiler gradient [100%] and a gap of 228 μsec to the start of the section-encoding gradients with off-resonance frequencies of 50–10000 Hz; direct saturation larger than 10000 Hz is negligible), a wait time of 1519 μsec, followed by a radiofrequency pulse (sinc shape; 12° angle; 1-msec duration with spoiler gradients of the imaging sequence starting 5986 μsec after the center of the excitation pulse; read spoiler duration, 1 msec [30%]; and section spoiler duration, 1.2 msec [40%]). This routine was repeated 512 times (reaching equilibrium typically at

80–100 iterations) by using previously published T1 and T2 values (18). Direct saturation effects (MT_{dir} in the following equation) were quantified as the reduction of transverse magnetization due to the MT pulse in the MR sequence $MT_{dir} = S_0 - S_{MT}/S_0$, with S_0 meaning the transverse magnetization after the first excitation and S_{MT} meaning the transverse magnetization after equilibration of the sequence. True MT (MT_{true}) was subsequently calculated from the experimental MTR by subtracting the direct saturation effects that resulted from direct saturation.

Histologic Examination to Assess Muscle Tissue Formation and Muscle Marker Expression

The mice were sacrificed 14 and 28 days after cell injection, and the tissue-engineered muscles were excised from their backs, frozen, and sectioned at 10 μm. Hematoxylin-eosin and Masson trichrome staining were performed with the frozen sections from the different time points to assess muscle tissue formation. For immunohistochemistry analysis, tissue sections were incubated with primary mouse antibody against human myosin heavy chain (MyHC) (1:1) overnight at 4°C and secondary rabbit antimouse antibody cyanine 3 immunoglobulin G (1:1000) together with 4′,6-diamidine-2-phenylindole·dihydrochloride (1:100) at room temperature for 1 hour.

Western Blot Analysis to Assess Muscle Marker Expression

Seven, 14, and 28 days after hMPC injection, the newly formed muscle tissues were harvested and frozen. For Western blot analyses, the samples were powderized in liquid nitrogen and lysed with lysis buffer that contained 50 mmol/L Tris-HCl, with a pH level of 7.4, 150 mmol/L NaCl, 10% glycerol, 1% Triton X-100 (Sigma), 2 mmol/L ethylenediaminetetraacetic acid, 50 mmol/L sodium fluoride, 200 μmol/L sodium orthovanadate, and protease inhibitor cocktail (Sigma-Aldrich). The total protein content of each lysate was quantified with the BCA Protein Assay Kit (Thermo Scientific, Lausanne, Switzerland), and 30 μg per sample was loaded on a 12% gel (Bio-Rad, Cressier, Switzerland). The separated proteins were electrotransferred onto a polyvinylidene fluoride membrane (Immobilion-P; Millipore, Bedford, Mass). The membranes were incubated with primary antibodies against MyHC (1:2, Developmental Studies Hybridoma Bank), α-actinin (1:2000, Sigma), desmin (1:500, Sigma), and monoclonal glyceraldehyde-3-phosphate dehydrogenase (1:2500, Sigma) in Tris-buffered saline with 0.1% Tween-20 (Sigma) and 5% nonfat dry milk overnight at 4°C. The membranes were subsequently washed and incubated with the appropriate horseradish peroxidase–conjugated secondary antibody (1:6000, Amersham Pharmacia Biotech, Dübendorf, Switzerland) in Tris-buffered saline and Tween 20 (Sigma) for 1 hour at room temperature. The signals on the membranes were detected by using the electrochemiluminescence method (ECL Kit, Amersham Pharmacia Biotech) and analyzed by using Image Studio Lite (Li-Cor, Lincoln, Neb) software, with the intensity of each band of interest being normalized to glyceraldehyde-3-phosphate dehydrogenase.

Myography to Assess Muscle Tissue Contractility

Contractility of the newly formed tissues was evaluated with myography 4 weeks after hMPC injection. The excised muscle strips were fastened with suture loops to the transducer in tissue bath chambers and were immersed in Krebs solution (119 mmol/L NaCl, 4.4 mmol/L KCl, 20 mmol/L $NaHCO_3$, 1.2 mmol/L NaH_2PO_4, 1.2 mmol/L $MgCl_2$, 2.5 mmol/L $CaCl_2$, and 11 mmol/L glucose) under constant oxygenation at room temperature. Muscle strips were treated with electrical field stimulation (40 Hz at 40 V and 80 Hz at 80 V), and contractions were recorded. The values were normalized to the sample weight (milligram per milligram of tissue).

Statistics

Experiments were repeated with at least three human samples. Data were analyzed by using one-way analysis of variance with the Sidak multiple comparisons test (for myography data) or two-way analysis of variance with the Tukey multiple comparisons test (for Western blot analysis data from one time point to all other time points for all proteins and days and for MTR values from one time point to all other time points for all offset frequencies and days). The results are presented as mean values ± standard deviations, and data with a P value less than .05 were considered to indicate a significant difference.

Results

Morphologic MR Imaging and MT Image Contrast

Typical MR imaging images of mice after hMPC transplantation are displayed in Figure E1 (online) at three different time points. T2-weighted images display the sites of injection and the subsequent decrease in injected volume over 28 days. Moreover, it can be seen that the signal intensities of the hMPCs decrease during differentiation, indicating a decrease in the respective T2 transverse relaxation time. On the MT images, it can be observed that the signal intensity of tissues decreases compared with the images without MT prepulse, except for fatty tissue. At low MT off-resonance frequency (50 Hz), this effect is predominantly caused by direct saturation (assessment of direct saturation is further described herein). At off-resonance frequencies of 1750 Hz and higher, true MT is visible with signal intensity primarily in the area of skeletal muscle. Regarding the signal intensity of the hMPCs, no change in signal intensity from day 1 to day 14 without application of an MT prepulse is visible. However, decreasing signal intensity when applying an MT prepulse can be observed from day 1 to day 14, irrespective of the chosen offset frequency. The acquired signal intensity further decreased from day 14 to day 28 with applied prepulse for all off-resonance frequencies; but also a minor change in signal intensity could be observed without prepulse (which is due to a change in the relaxation properties, as shorter

Figure 1

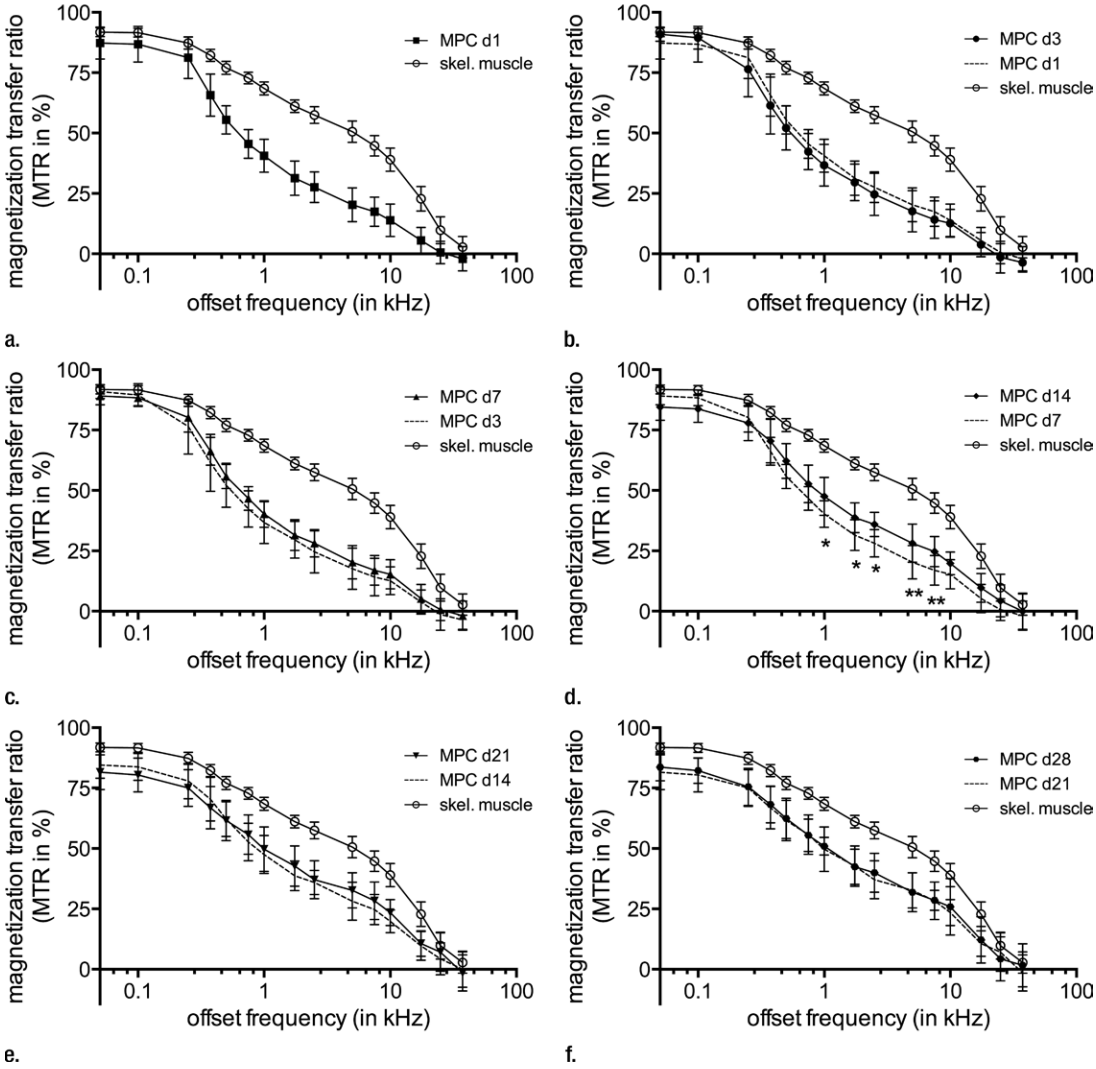

Figure 1: Graphs show MTR as a function of offset frequencies. hMPCs were injected into the subcutaneous space of nude mice and evaluated with MT MR imaging over the time course of 28 days. **(a)** Day 1, **(b)** day 3, **(c)** day 7, **(d)** day 14, **(e)** day 21, and **(f)** day 28 values are shown. MTR of hMPCs (n = 8–15) was plotted as a function of offset frequencies, and values of the previous time point (dashed line) were included in each graph to visualize progressive changes. Skeletal muscle (n = 43) was used as a reference. * = $P < .05$ (statistically significant) when compared with the previous time point, ** = $P < .01$ (statistically significant) when compared with the previous time point.

T2* time causes a signal intensity decrease with a gradient-echo sequence).

Validation of the MT Protocol and Sequence Simulation

The experimental setup of the MT MR imaging measurements was validated in phantom experiments with 4% agarose. The corresponding MTRs are depicted in Figure E2 (online). Highest MT ratios were observed for small off-resonance frequencies on the order of 100%. With increasing off-resonance frequency, the MT ratios exhibited a monotone decline asymptotically, reaching zero at off-resonance frequencies higher than 50 kHz. A characteristic shoulder can be seen at 2–20 kHz for 600° and 1200° flip angle.

The accuracy of the Bloch equation simulation was assessed by means of comparison to experimental MTR measurements in a water phantom. Since water does not show any MT, the signal intensity obtained must reflect pure direct saturation. An excellent correspondence between simulation and measurement data can be seen in Figure E3 (online).

Quantitative Evaluation of MT Ratios

Curves of the mean MT ratios in dependence of the off-resonance frequency are depicted in Figure 1 for hMPCs

Figure 2

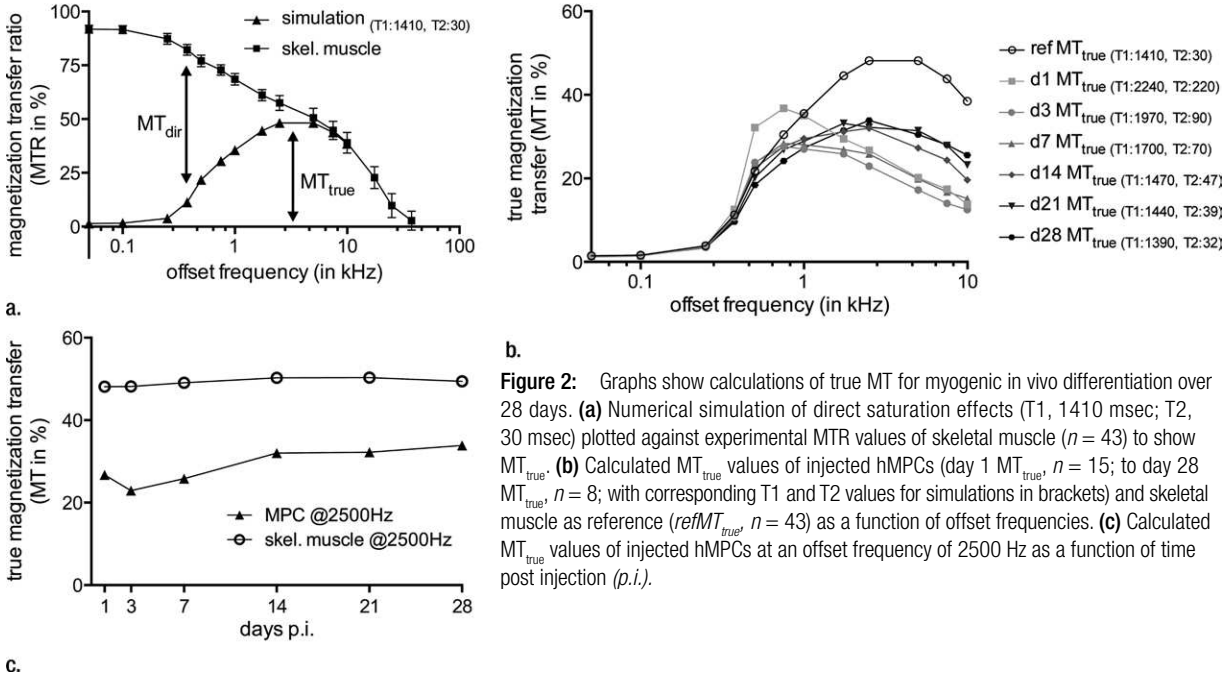

Figure 2: Graphs show calculations of true MT for myogenic in vivo differentiation over 28 days. **(a)** Numerical simulation of direct saturation effects (T1, 1410 msec; T2, 30 msec) plotted against experimental MTR values of skeletal muscle ($n = 43$) to show MT_{true}. **(b)** Calculated MT_{true} values of injected hMPCs (day 1 MT_{true}, $n = 15$; to day 28 MT_{true}, $n = 8$; with corresponding T1 and T2 values for simulations in brackets) and skeletal muscle as reference (*ref*MT_{true}, $n = 43$) as a function of offset frequencies. **(c)** Calculated MT_{true} values of injected hMPCs at an offset frequency of 2500 Hz as a function of time post injection *(p.i.)*.

and the reference of skeletal muscle at different time points during differentiation. MTR values of skeletal muscle displayed a gradual decrease from 91.8% ± 1.8 to 2.7% ± 4.4 with increasing offset frequencies, resulting in a maximal MTR of 57.5% ± 3.5 at 2500 Hz. At day 1, MTR values from 87.3% ± 6.7 to −2.0% ± 5.0 were observed for injections of hMPCs in collagen with increasing offset frequencies, demonstrating much lower values in the midrange of offset frequencies. At 2500 Hz, an MTR of 27.6% ± 6.3 for hMPCs was obtained at day 1. Interestingly, the MTR values showed a decrease from day 1 to day 3 (MTR, 24.7% ± 8.7 at 2500 Hz) but increased at the following time points to an MTR of 28.2% ± 5.7, 35.9% ± 5.0, 37.0% ± 7.9, and 39.9% ± 8.1 for days 7, 14, 21, and 28, respectively. Similar changes in MTR values could be observed for all offset frequencies between 500 and 17500 Hz. Notably, however, MTR values reached a plateau on day 21, being between 64% and 72% of the skeletal muscle reference, with little to no increase by day 28. The increase in MTR values from day 1 to days 3 or 7 was not significant. However, from days 1, 3, or 7 to day 14 (and later time points), a statistically significant increase (with $P < .05$ or better) could be seen. While MTR values increased from day 14 to day 21, this increase was not statistically significant. Only a small increase or no increase at all could be seen from day 21 to day 28.

Numerical simulations were used to subtract direct saturation effects from the measured MTR values to obtain MT_{true} (Fig 2). Experimental MTR values and calculated MT_{true} are shown for skeletal muscle (Fig 2a). Calculating MT_{true} for offset frequencies between 50 and 10000 Hz (upper limit of computation for direct saturation effects) demonstrated increasing values, reaching 48.2% at 2500 Hz before declining to 38.5% at 10000 Hz (Fig 2b). Interestingly, while similar changes in MT_{true} could be observed for injections of hMPCs in collagen with increasing offset frequencies, maximum values were observed at lower offset frequencies for earlier time points. Maximum MT_{true} was found to increase over time with 36.8% at 750 Hz, 27.6% at 750 Hz, 28.4% at 750 Hz, 32.0% at 2500 Hz, 32.2% at 2500 Hz, and 33.9% at 2500 Hz at days 1, 3, 7, 14, 21, and 28, respectively. The development of MT_{true} over time is shown for an offset frequency of 2500 Hz in Figure 2c, and values were found to reach 68.8% of the MT_{true} of skeletal muscle.

Injected hMPCs Form Functional Muscle Tissue

To evaluate the newly formed muscle tissue for correct morphologic appearance and function, histologic examination, immunohistochemistry analysis, Western blot analysis, and myography were performed at different time points.

Representative images of tissue sections from two different experiments at days 14 and 28 that were stained with hematoxylin-eosin, Masson trichrome, or, for a specific muscle marker, MyHC, are shown in Figure E4 (online). Collagenous tissue or a mix of collagenous tissue and muscle fibers could be observed at day 14, with an increasing amount of muscle fibers apparent by day 28. Muscle fiber formation was confirmed with MyHC staining. Skeletal muscle was used as a reference, showing nicely

aligned muscle fibers that showed positive staining for MyHC.

Western blot of the injected hMPCs with collagen was performed at days 7, 14, and 28 for muscle-specific proteins MyHC, α-actinin, and desmin, as well as for glyceraldehyde-3-phosphate dehydrogenase as a reference protein (Fig E5a [online]). All muscle-specific proteins could be detected, displaying lower protein expression at day 7 and day 14 but much stronger expression at day 28. This increased expression was statistically significant for desmin between day 7 and day 28 but not for the other proteins.

Myography was performed at day 28 to evaluate contractility as a measure of tissue functionality (Fig E5b [online]). Two different electrical regimens (40 V and 40 Hz; and 80 V and 80 Hz) were used to monitor contraction levels of bioengineered muscle tissues with collagen-only and skeletal muscle (tibialis anterior) as a reference. Engineered muscle tissue displayed contraction levels that reached 13%–16% of the skeletal muscle reference.

Discussion

MT describes the interaction of tissue-water protons that reside in different environments, encompassing the "free" water proton pool responsible for the conventional MR imaging signal intensity and the "restricted" proton pool where protons are bound to macromolecules (25). Owing to the large abundance of macromolecules in the form of aligned muscle fibers in well-developed muscle tissue, muscle shows higher MT than most other tissues of the human body. Therefore, MT could represent an ideal biomarker for characterization of fiber formation during muscle development. Importantly, no MT is found in water because of the lack of macromolecules for interaction; also, fatty tissue does not show MT because of a lack of mobile water molecules.

In our study, in vivo myogenic differentiation of hMPCs in mice was monitored with MT MR imaging, and muscle formation was confirmed by histologic findings, Western blot analysis, and measurement of tissue contractility. Experimental MT measurements were validated by using a previously described agarose model (26). Both MTR values and MT_{true} (subsequently referred to as "MT values") increased over the investigated time period of 28 days, reaching a plateau at day 21 with around 70% of native skeletal muscle. This increase was, however, only observed after an initial decrease from day 1 to day 3. The initially higher MT values at day 1 are probably due to the high collagen content used for injection of the hMPCs. This is supported by previous work on monitoring of intestinal fibrosis of Crohn disease (27), as well as a study on pancreatic cancer xenografts (28), which demonstrated a correlation of collagen content and high MTR values. The decrease of MT values from day 1 to day 3 is likely due to initial remodeling and degradation of the injected collagen, and only after day 3 do changes in MT values reflect the process of muscle fiber formation from injected hMPCs.

Interestingly, MT values increased from day 3 to day 21; however, not much change could be observed from day 21 to day 28. Reasons for these observations can be manifold, but incomplete muscle tissue formation and an unorganized tissue structure are likely to be major contributors. This is supported by histologic results, which show larger areas of collagenous tissue along or in between newly formed muscle fibers at 14 and 28 days. Also, tissue contractility assessed via myography demonstrated that contraction levels of hMPC-derived muscle tissue reaches only about 13%–16% of native muscle by day 28, which is, however, much lower compared with the observations with MT MR imaging (MT values reached around 70% those of native muscle). This discrepancy can possibly be explained by the large differences in the structural organization of the assessed tissue samples. The skeletal muscle reference (tibialis anterior) consists of nicely aligned, densely packed muscle fibers and allows fixation of the muscle for myography in correct orientation by using the ligaments. The bioengineered muscle tissue from our study, on the other hand, consists of nonoriented fibers and remains of collagenous tissue, where no correct orientation for fixation exists. While this is probably due to injections in the subcutaneous space without structural guidance for oriented muscle fiber formation, it is possibly less relevant if hMPCs are injected into damaged muscle tissue, as remaining tissue still provides some guidance for newly forming muscle fibers. Supporting this, it could be shown previously in a large animal model that when autologous hMPCs are injected into the damaged sphincter muscle, 80% of the initial sphincter pressure can be restored (11). Finally, evaluating different offset frequencies of the MT prepulse, the range between 2500 and 5000 Hz could be defined to give optimal MT image contrast, which is in good agreement with previous findings (29). A decrease in signal intensity was observed with the sequence without prepulse from day 14 to day 28, which reflects the shortening of the T2* time of the tissue, presumably due to lower water content. This decrease was considered in the calculation of the direct saturation effects by adjustment of the respective relaxation properties in the Bloch simulation. Therefore, the change in relaxation properties did not negatively affect the MT quantification accuracy, which is also supported by the stability of MTR between day 14 and day 28.

Our study had limitations. First, T1 and T2 relaxation time measurements, which are required for estimation of direct saturation effects, could not be performed in the same session as MT experiments because of the constraints regarding measurement time of the nude mice in one session; instead, T1 and T2 data from previous studies have been used. Second, only a phenomenological description of the observed MT effects with increasing fiber content is provided. We did not investigate the chemical basis of the effect (eg, the chemical exchange processes taking place between macromolecular and liquid pool).

In conclusion, MT MR imaging may be used to noninvasively monitor the process of myogenic in vivo

differentiation of hMPCs as a biomarker of the quantity and quality of muscle fiber formation. While previous measurements of relaxation properties presented identical values for hMPC-derived muscle tissue and native muscle (18), our results based on MT values ultimately allow for evaluation of muscle tissue quality. On the basis of our findings, application of sophisticated MR imaging techniques seems to hold great promise in enabling clinical evaluation of the success of cell therapy approaches.

Acknowledgments: We thank the Clinical Research Priority Program (KFSP) Molecular Imaging Network Zurich (MINZ) for financial support.

Disclosures of Conflicts of Interest: M.R. disclosed no relevant relationships. **D.H.** disclosed no relevant relationships. **S.S.** disclosed no relevant relationships. **C.E.** disclosed no relevant relationships. **M.C.W.** disclosed no relevant relationships. **A.B.** disclosed no relevant relationships. **D.E.** disclosed no relevant relationships.

References

1. Holroyd-Leduc JM, Straus SE. Management of urinary incontinence in women: scientific review. JAMA 2004;291(8):986–995.
2. Brown JS, Nyberg LM, Kusek JW, et al. Proceedings of the National Institute of Diabetes and Digestive and Kidney Diseases International Symposium on Epidemiologic Issues in Urinary Incontinence in Women. Am J Obstet Gynecol 2003;188(6):S77–S88.
3. Wilson L, Brown JS, Shin GP, Luc KO, Subak LL. Annual direct cost of urinary incontinence. Obstet Gynecol 2001;98(3):398–406.
4. Atala A. Tissue engineering for the replacement of organ function in the genitourinary system. Am J Transplant 2004;4(Suppl 6):58–73.
5. De Filippo RE, Yoo JJ, Atala A. Engineering of vaginal tissue in vivo. Tissue Eng 2003;9(2):301–306.
6. Kang SB, Lee HN, Lee JY, Park JS, Lee HS, Lee JY. Sphincter contractility after muscle-derived stem cells autograft into the cryo-injured anal sphincters of rats. Dis Colon Rectum 2008;51(9):1367–1373.
7. Leobon B, Garcin I, Menasche P, Vilquin JT, Audinat E, Charpak S. Myoblasts transplanted into rat infarcted myocardium are functionally isolated from their host. Proc Natl Acad Sci U S A 2003;100(13):7808–7811.
8. Yiou R, Yoo JJ, Atala A. Restoration of functional motor units in a rat model of sphincter injury by muscle precursor cell autografts. Transplantation 2003;76(7):1053–1060.
9. Chancellor MB, Yokoyama T, Tirney S, et al. Preliminary results of myoblast injection into the urethra and bladder wall: a possible method for the treatment of stress urinary incontinence and impaired detrusor contractility. Neurourol Urodyn 2000;19(3):279–287.
10. Yokoyama T, Huard J, Pruchnic R, et al. Muscle-derived cell transplantation and differentiation into lower urinary tract smooth muscle. Urology 2001;57(4):826–831.
11. Eberli D, Aboushwareb T, Soker S, Yoo JJ, Atala A. Muscle precursor cells for the restoration of irreversibly damaged sphincter function. Cell Transplant 2012;21(9):2089–2098.
12. Carr LK, Robert M, Kultgen PL, et al. Autologous muscle derived cell therapy for stress urinary incontinence: a prospective, dose ranging study. J Urol 2013;189(2):595–601.
13. Fu Y, Azene N, Xu Y, Kraitchman DL. Tracking stem cells for cardiovascular applications in vivo: focus on imaging techniques. Imaging Med 2011;3(4):473–486.
14. Azzabi F, Rottmar M, Jovaisaite V, et al. Viability, differentiation capacity, and detectability of super-paramagnetic iron oxide-labeled muscle precursor cells for magnetic-resonance imaging. Tissue Eng Part C Methods 2015;21(2):182–191.
15. Rivière C, Lecoeur C, Wilhelm C, et al. The MRI assessment of intraurethrally—delivered muscle precursor cells using anionic magnetic nanoparticles. Biomaterials 2009;30(36):6920–6928.
16. Prompers JJ, Jeneson JA, Drost MR, Oomens CC, Strijkers GJ, Nicolay K. Dynamic MRS and MRI of skeletal muscle function and biomechanics. NMR Biomed 2006;19(7):927–953.
17. Theodorou DJ, Theodorou SJ, Kakitsubata Y. Skeletal muscle disease: patterns of MRI appearances. Br J Radiol 2012;85(1020):e1298–e1308.
18. Chuck NC, Azzabi Zouraq F, Rottmar M, Eberli D, Boss A. MR imaging relaxometry allows noninvasive characterization of in vivo differentiation of muscle precursor cells. Radiology 2015;274(3):800–809.
19. Boss A, Martirosian P, Küper K, Fierlbeck G, Claussen CD, Schick F. Whole-body magnetization transfer contrast imaging. J Magn Reson Imaging 2006;24(5):1183–1187.
20. Petrella JR, Grossman RI, McGowan JC, Campbell G, Cohen JA. Multiple sclerosis lesions: relationship between MR enhancement pattern and magnetization transfer effect. AJNR Am J Neuroradiol 1996;17(6):1041–1049.
21. Pazahr S, Blume I, Frei P, et al. Magnetization transfer for the assessment of bowel fibrosis in patients with Crohn's disease: initial experience. MAGMA 2013;26(3):291–301.
22. McDaniel JD, Ulmer JL, Prost RW, et al. Magnetization transfer imaging of skeletal muscle in autosomal recessive limb girdle muscular dystrophy. J Comput Assist Tomogr 1999;23(4):609–614.
23. Eberli D, Soker S, Atala A, Yoo JJ. Optimization of human skeletal muscle precursor cell culture and myofiber formation in vitro. Methods 2009;47(2):98–103.
24. Springer F, Steidle G, Martirosian P, Claussen CD, Schick F. Effects of in-pulse transverse relaxation in 3D ultrashort echo time sequences: analytical derivation, comparison to numerical simulation and experimental application at 3T. J Magn Reson 2010;206(1):88–96.
25. Henkelman RM, Huang X, Xiang QS, Stanisz GJ, Swanson SD, Bronskill MJ. Quantitative interpretation of magnetization transfer. Magn Reson Med 1993;29(6):759–766.
26. Henkelman RM, Stanisz GJ, Graham SJ. Magnetization transfer in MRI: a review. NMR Biomed 2001;14(2):57–64.
27. Adler J, Swanson SD, Schmiedlin-Ren P, et al. Magnetization transfer helps detect intestinal fibrosis in an animal model of Crohn disease. Radiology 2011;259(1):127–135.
28. Li W, Zhang Z, Nicolai J, Yang GY, Omary RA, Larson AC. Magnetization transfer MRI in pancreatic cancer xenograft models. Magn Reson Med 2012;68(4):1291–1297.
29. Stanisz GJ, Odrobina EE, Pun J, et al. T1, T2 relaxation and magnetization transfer in tissue at 3T. Magn Reson Med 2005;54(3):507–512.